# Urban Surface Biophysical Descriptors and Land Surface Temperature Variations

**Qihao Weng, Dengsheng Lu, and Bingqing Liang**

## Abstract

*In remote sensing studies of land surface temperatures (LST), thematic land-use and land-cover (LULC) data are frequently employed for simple correlation analyses between LULC types and their thermal signatures. Development of quantitative surface descriptors could improve our capabilities for modeling urban thermal landscapes and advance urban climate research. This study developed an analytical procedure based upon a spectral unmixing model for characterizing and quantifying the urban landscape in Indianapolis, Indiana. A Landsat Enhanced Thematic Mapper Plus image of the study area, acquired on 22 June 2002, was spectrally unmixed into four fraction endmembers, namely, green vegetation, soil, high and low albedo. Impervious surface was then computed from the high and low albedo images. A hybrid classification procedure was developed to classify the fraction images into seven land-use and land-cover classes. Next, pixel-based LST measurements were related to urban surface biophysical descriptors derived from spectral mixture analysis (SMA). Correlation analyses were conducted to investigate land-cover based relationships between LST and impervious surface and green vegetation fractions for an analysis of the causes of LST variations. Results indicate that fraction images derived from SMA were effective for quantifying the urban morphology and for providing reliable measurements of biophysical variables such as vegetation abundance, soil, and impervious surface. An examination of LST variations within census block groups and their relationships with the compositions of LULC types, biophysical descriptors, and other relevant spatial data shows that LST possessed a weaker relation with the LULC compositions than with other variables (including urban biophysical descriptors, remote sensing biophysical variables, GIS-based impervious surface variables, and population density). Further research should be directed to refine spectral mixture modeling. The use of multi-temporal remote sensing data for urban time-space modeling and comparison of urban morphology in different geographical settings are also feasible.*

## Introduction

The receipt and loss of radiation of urban surfaces correspond closely to the distribution of land-use and land-cover (LULC) characteristics. Because of this correspondence, there has been a tendency to use thematic LULC data, not quantitative surface descriptors, to describe urban thermal landscapes (Voogt and Oke, 2003). This trend of qualitative description of thermal patterns and simple correlations between LULC types and their thermal signatures has slowed down the development of remote sensing of land surface temperature (LST) and thus surface temperature heat islands (Voogt and Oke, 2003). Clapham (2003) suggests using of a continuum-based classification for satellite imagery, which aims to provide continuous data for the "functional classes." The idea of a continuum-based classification has long been pursued in urban landscape analysis. One of the major contributions is Ridd's (1995) vegetation-impervious surface-soil (V-I-S) model for characterizing urban environments. This model assumes that urban land-cover is a linear combination of three biophysical components: vegetation, impervious surface, and soil, and has recently been successfully implemented by using the technique of spectral mixture analysis (Ward *et al.*, 2000; Madhavan *et al.*, 2001; Rashed *et al.*, 2001; Small, 2001; Phinn *et al.*, 2002; Wu and Murray, 2003, Lu and Weng, 2004). The Ridd model provides the potential for a link between remote sensing-derived urban biophysical components and LST, and may be applied to establish parameters for describing urban construction materials and fabrics to improve our understanding of urban surface energy budget and heat islands.

The focus of this research is placed on the development of a methodology to examine the interplay between LST and urban morphology. A Landsat ETM+ image of 2000 that covers the City of Indianapolis, Indiana was used in conjunction with other types of spatial data for the analysis. Specific objectives of this research are: (a) to employ spectral mixture modeling to derive urban surface biophysical attributes, and to apply spectrally unmixed results to characterize the urban landscape; (b) to analyze the causes of LST variations, which were derived from Landsat thermal infrared data by linking LST with remotely sensed urban surface descriptors; and (c) to examine the spatial variations of LST at the census block group level, so that implications for urban planning may be explored.

The City of Indianapolis, located in Marion County, Indiana (Figure 1), is the nation's twelfth largest city, with approximately 0.8 million population (over 1.6 million in the metropolitan area). Situated in the middle of the country, Indianapolis possesses several other advantages that make it an appropriate choice. It has a single central city, and other large urban areas in the vicinity have not

Qihao Weng and Bingqing Liang are with the Department of Geography, Geology, and Anthropology, Indiana State University, Terre Haute, IN 47809 (geweng@isugw.indstate.edu).

Dengsheng Lu is with the Center for the Study of Institutions, Population, and Environmental Change, Indiana University, Bloomington, IN 47408 (dlu@indiana.edu).

Photogrammetric Engineering & Remote Sensing
Vol. 72, No. 11, November 2006, pp. 1275–1286.

0099-1112/06/7211–1275/$3.00/0

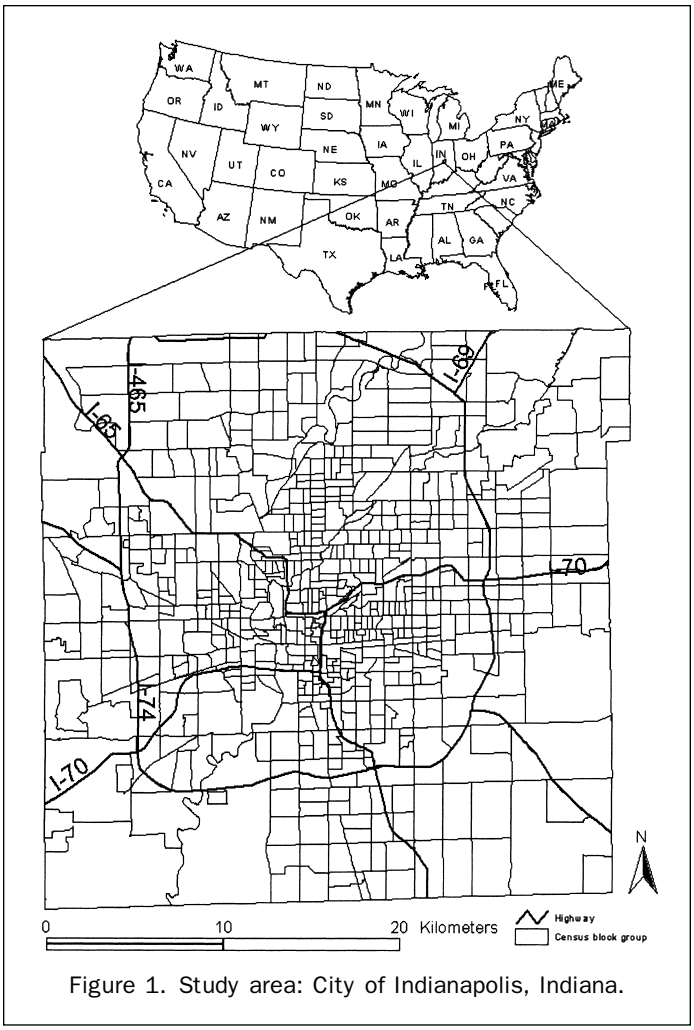


Figure 1. Study area: City of Indianapolis, Indiana.

influenced its growth. The city is located on a flat plain and is relatively symmetrical, having possibilities of expansion in all directions. Like most American cities, Indianapolis is increasing in population and in area. The areal expansion is through encroachment into the adjacent agricultural and non-urban land. Certain decision-making forces have encouraged some sectors of Metropolitan Indianapolis to expand faster than others. Detecting and analyzing its urban thermal landscape is significant to control and plan the city's future development.

## Thermal Remote Sensing of Urban Surface Temperatures

In urban areas, natural vegetation is often removed and replaced by non-evaporating, non-transpiring impervious surfaces. Under such alteration, the partitioning of incoming solar radiation into fluxes of sensible and latent heat is skewed in favor of increased sensible heat flux as evapotranspirative surfaces are reduced. A higher level of latent heat exchange is found with more vegetated areas, while sensible heat exchange is more favored by sparsely vegetated urban areas that have large amounts of impervious surfaces (Oke, 1982). The LST pattern is a manifestation of existing surface energy balance and has been extensively studied with thermal remote sensing technology.

Satellite thermal infrared sensors measure top of the atmosphere (TOA) radiances from which brightness temperatures of land surfaces (also known as blackbody temperatures) can be derived using Plank's law (Dash *et al.*, 2002). The difference between the TOA and land surface brightness temperatures ranges generally from 1 K to 5 K in the 10 to 12 $\mu$m spectral region, subject to the influence of the atmospheric conditions (Prata *et al.*, 1995). Research on LST shows that the partitioning of heat fluxes and thus surface energy response is a function of varying surface soil water content and vegetation cover (Owen *et al.*, 1998). For non-vegetated areas, LST measurements typically represent the radiometric temperatures of sunlit surfaces, such as bare soil and impervious surface. As the amount of vegetation cover increases, the radiative temperature recorded by a sensor approximates more closely the temperatures of green leaves and the canopy temperature at spectral vegetation maximum or complete canopy cover (Goward *et al.*, 2002). The observed portion of vegetation and non-vegetation surfaces can vary with the viewing angle, thus the amount of vegetation (ground) alters as the observation angle increases (Caselles *et al.*, 1992a and 1992b).

Generally speaking, LST are a function of four surface and subsurface properties: albedo, emissivity, thermal properties of urban construction materials, and the composition and structure of urban canopy (Goward, 1981). Moisture is included in the thermal properties of materials. Each of these characteristics displays a wide range of variation in urban contexts. Following discussion focuses on the relationship between LST and the three urban landscape components identified in the Ridd model: vegetation, impervious surface, and soil.

Fractional vegetation cover depicts the amount and nature of vegetation cover, and modulates the proportions of vegetation and ground visible to a sensor. The relationship between LST and vegetation cover has been extensively studied by using vegetation indices such as the Normalized Difference Vegetation Index (NDVI). However, the relationship between NDVI and fractional vegetation cover is not singular. A recent study indicates that NDVI does not provide areal estimates of the amount of vegetation (Small, 2001). Plant species, leaf area, soil background, and shadow may all contribute to the NDVI variability (Jasinski, 1990). More quantitative, physically based measures of vegetation abundance are called for, especially for applications that require biophysical measures (Small, 2001). Weng *et al.* (2004) found that LST possessed a slightly stronger negative correlation with vegetation fraction derived from a spectral mixture modeling, than with NDVI for all LULC types across the spatial resolution from 30 to 960 meters.

Impervious surfaces refer to two major functional categories of urban surfaces: rooftops and the transportation system (roads, parking lots, driveways, and sidewalks) (Schueler, 1994). Impervious surfaces trigger local decreases in infiltration, percolation and soil moisture, reductions in natural interception and depression storage and increases in runoff (Brun and Band, 2000). As a result, impervious surfaces in the urban context experience an almost dichotomous wet/dry behavior, affecting local partitioning of daytime radiant energy (Oke, 1982). The surface energy balance of impervious surfaces is characterized by partitioning of the net radiance into sensible heat and heat conducted to the substrate (i.e., storage heat flux) (Oke, 1982). The energy balance systems may vary considerably with site geometries and construction materials. The influence of geometry may vary with the changes in building density, height, and size, and street canyon orientation. High-rise buildings are found to be cooler than low-rise buildings and non-built areas because the latter have a greater portion of active horizontal surface and low buildings cast shorter shadows, while smaller buildings with smaller building mass tend to have lower thermal inertia, leading to a quicker heat accumulation during the daytime (Nichol, 1996).

For any surface material, certain internal properties, such as heat capacity, thermal conductivity and inertia, play important roles in governing the temperature of a body at equilibrium with its surroundings (Campbell, 2002). These thermal properties vary with soil type and its moisture content (Sandholt *et al.*, 2002). Dry, bare, and low-density soils, for example, are linked to high LST owing to relatively low thermal inertia (Carnahan and Larson, 1990). The emissivity of soils is a function of soil moisture conditions, and soil density (Larson and Carnahan, 1997).

## Methods

### Image Pre-processing

Landsat 7-Enhanced Thematic Mapper Plus (ETM+) image (Row/Path: 32/21) dated on 22 June 2000 was used in this research. The data acquisition date has a highly clear atmospheric condition, and the image was acquired through the USGS Earth Resource Observation Systems Data Center, which has corrected radiometric and geometrical distortions of the image to a quality level of 1G before delivery. The Landsat image was further rectified to a common Universal Transverse Mercator coordinate system based on 1:24000 scale topographic maps, and was resampled using the nearest neighbor algorithm with a pixel size of 30 m by 30 m for all bands including the thermal band. The resultant root mean square error (RMSE) was found to be less than 0.5 pixel.

### Spectral Mixture Analysis

Linear Spectral Mixture Analysis (LSMA) is a physically-based image processing method. It assumes that the spectrum measured by a sensor is a linear combination of the spectra of all components within the pixel (Adams *et al.*, 1995; Roberts *et al.*, 1998a). The mathematical model of LSMA can be expressed as:

$$R_i = \sum_{k=1}^{n} f_k R_{ik} + ER_i \quad (1)$$

where $i = 1, \ldots, m$ (number of spectral bands); $k = 1, \ldots, n$ (number of endmembers); $R_i$ is the spectral reflectance of band $i$ of a pixel which contains one or more endmembers; $f_k$ is the proportion of endmember $k$ within the pixel; $R_{ik}$ is the known spectral reflectance of endmember $k$ within the pixel on band $i$; and $ER_i$ is the error for band $i$. Endmembers are recognizable land-cover materials/features that have homogenous spectral properties all over the image. A constrained least-squares solution was used in this research, assuming that the following two conditions are satisfied simultaneously:

$$\sum_{k=1}^{n} f_k = 1 \text{ and } 0 \le f_k \le 1 \quad (2)$$

$$\text{RMSE} = \sqrt{\left(\sum_{i=1}^{m} ER_i^2\right)/m} \quad (3)$$

Estimation of endmember fraction images with LSMA involves (a) image processing, (b) endmember selection, and (c) unmixing solution and evaluation of fraction images. Of these steps, selecting suitable endmembers is the most critical one in the development of high quality fraction images. Two types of endmembers can be applied: image endmembers, and reference endmembers. The former are derived directly from the image itself, while the latter are derived from field measurements or laboratory spectra of known materials (Roberts *et al.*, 1998a). For most remote sensing applications, image endmembers are utilized, since they are easily obtained and capable of representing the spectra measured at the same scale as the image data (Roberts *et al.*, 1998a). Image endmembers are derived from the extremes of the image feature space, based on the assumption that they represent the purest pixels in the image (Roberts *et al.*, 1998a; Mustard and Sunshine, 1999).

After the implementation of atmospheric correction and geometrical rectification of the ETM+ image, principal component analysis (PCA) was used to convert the ETM+ bands 1 through 5 and 7 into principal components. It is found that most of the information content was concentrated in the first three components (accounting for proximately 99 percent of the total variance). The scatter plots of PC1-PC2 and PC2-PC3 (Figure 2) were constructed to identify endmembers. Four endmembers, namely, high albedo, low albedo, soil, and green vegetation (GV), were selected. Figure 3 shows the spectral reflectance characteristics of these endmembers. A constrained least-squares solution was applied to compute four fraction images (Figure 4).

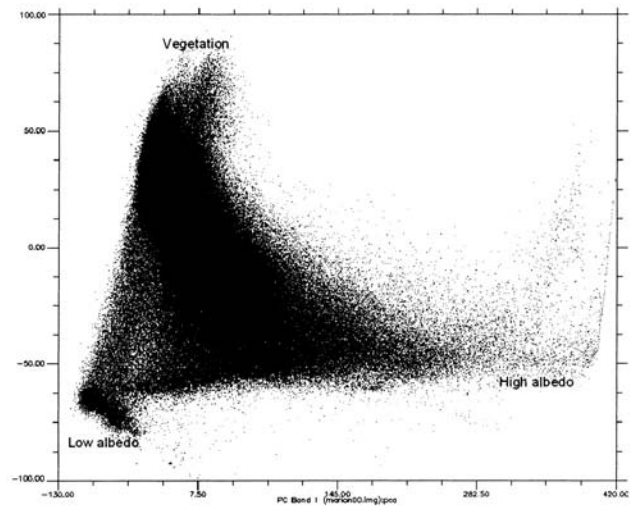


Figure 2. Scatterplots of principal components showing the locations of potential endmembers: (a) PCA 1 (*x*-axis) and PCA 2 (*y*-axis), and (b) PCA 2 (*x*-axis) and PCA 3 (*y*-axis).

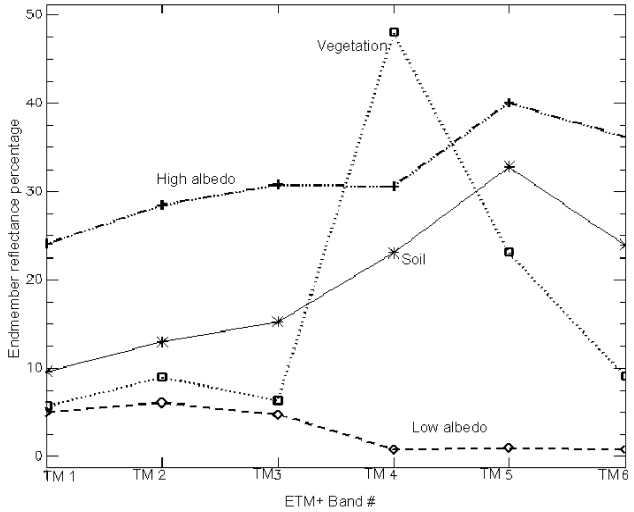


Figure 3. Spectral reflectance characteristics of the selected endmembers.

#### Impervious Surface Estimation

Impervious surface was estimated based on the spectral relationship between high and low albedo fractions and impervious surfaces following a procedure developed by Wu and Murray (2003). Before developing an impervious surface image, impacts from low reflectance materials (e.g., water and shade) and high reflectance materials (e.g., clouds and sand) were isolated and removed. Green vegetation and soil endmembers were considered not to contribute to impervious surface estimation. After removing these pixels, a pure impervious surface was calculated with low and high albedo endmembers by using a fully constrained linear mixture model (Figure 5). Our analysis indicated that the majority of commercial and industrial areas in the central business district had greater than 75 percent of impervious surface and rural areas near zero. The residential areas had a range from 25 percent to 75 percent of impervious surface.

#### Land-use and Land-cover Classification

The fraction images were used for LULC classification using a hybrid procedure that combined maximum likelihood and decision tree algorithms. A total of 156 sample plots were identified from high spatial resolution aerial photographs, covering initially ten LULC types: commercial and industrial, high-density residential, low-density residential, bare soil, crop, grass, pasture, forest, wetland, and water. On average, 10 to 16 sample plots for each class were selected. A window size of three by three was applied to extract the fraction value for each plot. The mean and standard deviation values were calculated for each LULC class. The characteristics of fractional composition for selected LULC types were then examined. Next, the maximum likelihood classification algorithm was applied to classify the fraction images into ten classes, generating a classified image and a distance image. A distance threshold was selected for each class to screen out the pixels that probably do not belong to that class and was determined by examining interactively the histogram of each class in the distance image. Pixels with a distance value greater than the threshold were assigned a class value of zero in the thematic image. A distance tree classifier was then applied to reclassify these pixels. The parameters required by the distance tree classifier were identified based on the mean and standard deviation from the sample plots of each class. Finally, the accuracy of the classified image was checked with a stratified random sampling method against the reference data of 150 samples collected from large-scale aerial photographs. Seven LULC types were identified, including: (a) commercial and industrial urban land, (b) residential land, (c) cropland, (d) grassland, (e) pasture, (f) forest, and (g) water. An overall accuracy of 89 percent and a Kappa index of 0.8575 were determined.

#### Estimation of LST

LSTs were derived from radiometrically and geometrically corrected ETM+ TIR band (10.44 to 12.42 $\mu$m). The ETM+ thermal band has a spatial resolution of 60 meters, and the thermal imagery from Landsat-7 is generally well-calibrated to ground truth data (Arvidson, 2002). The local time of satellite overpass was in the morning (approximately 1114). After converting the digital numbers (DN) of the ETM+ Band 6 into absolute radiance values, at-satellite brightness temperatures (i.e., blackbody temperature, $T_B$) were computed under an assumption of unity emissivity and using pre-launch calibration constants (Landsat Project Science Office, 2002). Next, correction for spectral emissivity ($\varepsilon$) was conducted according to the nature of land-cover. Each of the LULC categories was assigned an emissivity value by reference to the emissivity classification scheme proposed by Snyder *et al.* (1998). The emissivity corrected LSTs were computed using Equation 4 (Artis and Carnhan, 1982).

$$\mathrm{LST} = \frac{T_B}{1+(\lambda * T_B/\rho)\ln\varepsilon} \tag{4}$$

where: $\lambda$ = wavelength of emitted radiance (for which the peak response and the average of the limiting wavelengths ($\lambda$ = 11.5 $\mu$m) (Markham and Barker, 1985) will be used), $\rho$ = h * c/$\sigma$ (1.438*$10^{-2}$ m K), $\sigma$ = Boltzmann constant (1.38 * $10^{-23}$ J $K^{-1}$), h = Planck's constant (6.626*$10^{-34}$ J sec), and c = velocity of light (2.998 * $10^{8}$ m $s^{-1}$). The effects of atmosphere and surface roughness on LST were not taken into account in this study. Lack of atmospheric correction may introduce a temperature error of 4° to 7 °C for the mid-latitude summer atmosphere (Voogt and Oke, 1998). The magnitude of atmospheric correction depends upon image bands used as well as atmospheric conditions and the height of observation. However, the horizontal variation could have been minimized, because this study used an image acquired in a highly clear day and covering a small area. Errors due to urban effective anisotropy depend upon surface structure and relative sensor position, and can yield a temperature difference of up to 6 K or higher in downtown areas (Voogt and Oke, 1998).

## Results

#### Urban Surface Biophysical Descriptors

Figure 4 shows the four fraction images created, GV, soil, high albedo, and low albedo. An impervious surface fraction (Figure 5) was created by combining high and low albedo fraction images. Pixel values of a fraction image represented areal proportions of each biophysical descriptor within a pixel. GV fraction image showed a large dark area (low values) at the center of the study area that corresponds to the central business district of the city. Bright areas of high GV values were found in the surrounding areas. Various types of crops were still at the early stage of growth or were before emergence, as evidenced by medium gray to dark tone of the GV fraction image in the southeastern and southwestern parts of the city. Table 1 displays GV fraction values by LULC type. Forest apparently had the highest GV fraction values (0.715), followed by grassland (0.370). In

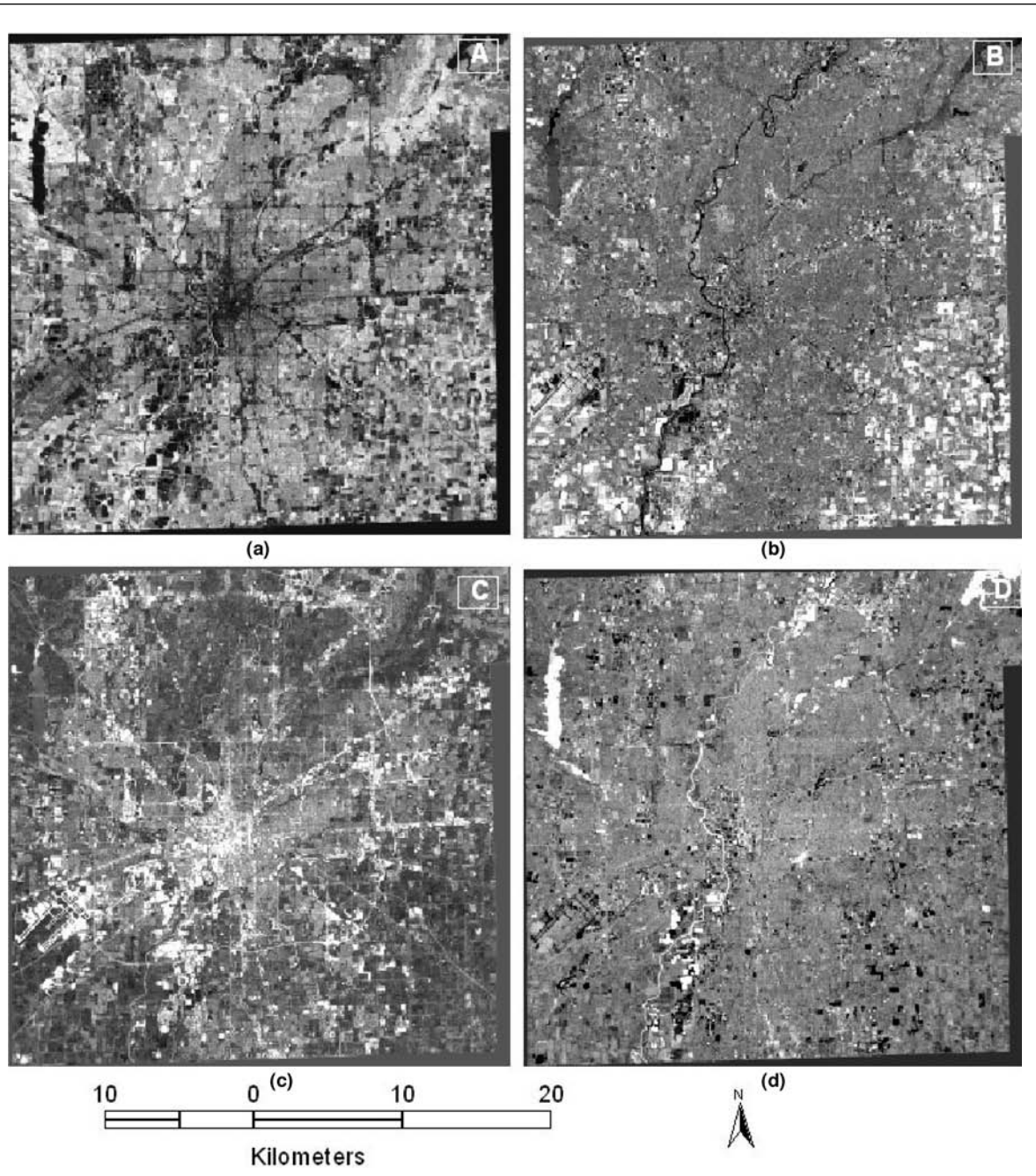


Figure 4. Fraction images derived from spectral mixture analysis of the Landsat ETM+ image: (a) vegetation, (b) soil, (c) high albedo, and (d) low albedo.

contrast, commercial and industrial land displayed the lowest GV values (0.119). Little vegetative amount was found in water bodies, as indicated by the GV fraction value (0.161). Residential land, pasture, and cropland yielded a mediate GV fraction value around 0.25. Residential land GV was slightly higher value than that of pasture and cropland. Cropland standard deviation was the highest, suggesting that cropland may be characterized by various amounts of vegetation coverage.

The percentage of land covered by impervious surfaces may vary significantly with LULC categories and sub-categories (Soil Conservation Service, 1975). This study shows a substantially different estimate for each LULC type, as this study applied a spectral unmixing model to the remote sensing images, and the modeling had introduced some errors. For example, a negative impervious fraction value was found in water. Generally speaking, a LULC type with a higher GV fraction appeared to have a lower impervious fraction. The highest impervious coverage was discovered in commercial and industrial land with a value of 0.491 (Table 1). Residential land ranked second, with a fraction value of 0.254. Grassland, pasture, and cropland returned a lower value of impervious surface ranging from 0.11 to 0.14, owing largely to their exposed bare soil, confusion with commercial and residential land, and computational errors. Forestland received a minimal impervious fraction value below 0.1.

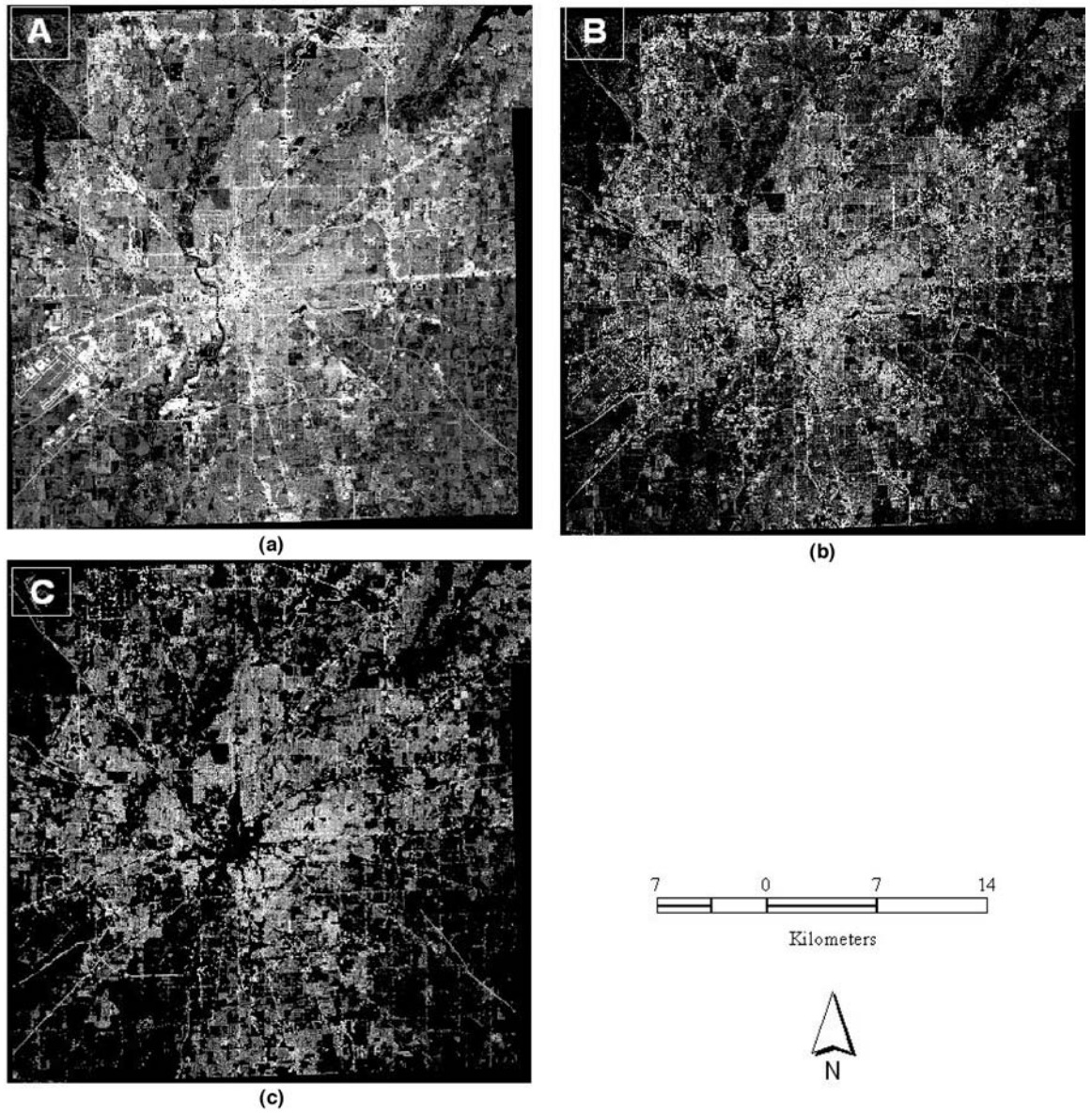


Figure 5. Impervious surface image derided from high-albedo and low-albedo fractions: (a) impervious surface, (b) adjusted impervious surface in which those pixel values greater than 75 percent or less than 25 percent were masked out, and (c) residential impervious surface in which those pixels of non-residential area were masked out.

Soil fraction values were generally low in the majority of the urban area, but high in the surrounding areas. Especially, in agricultural fields located in the southeastern and southwestern parts of the city, the soil fraction image was very bright since various types of crops were still at the early stage of growth. Table 1 shows that both pasture and cropland observed a high fraction value (pasture: 0.373; cropland: 0.3). Grassland possessed a medium fraction value of 0.211. Built-up lands, including residential, commercial and industrial land, displayed substantially lower soil fractions with 0.147 and 0.101, respectively. A minimal amount of soil was detected in forestland (fraction: 0.01). Water had a negative fraction value. Like GV fraction, soil fraction displayed the highest standard deviation value in cropland due to various amount of emerged vegetation.

The V-I-S composition may be examined by taking samples along transects. Figure 6 show ternary plots of two transects running across the geometric center of the city: sample 1 from west to east; and sample 2 from north to south. Errors from the spectral unmixing modeling are not included in these diagrams due to their low values clustering to near zero. Along the east to west transect, nearly all pixels sampled showed a GV fraction of less than 0.8, but the majority were in the range of 0.3 to 0.65. Soil fraction values were mostly below 0.4. A clustering pattern was apparent, if impervious fraction values were observed in the range from 0.2 to 0.6. However, a considerable number of pixels exhibited a high impervious fraction, having the fraction value up to 1.0. Sample 2 exhibited a more dispersed pattern of pixel distribution, suggesting a variety of V-I-S composition types. Pixels along the transect yielded a

TABLE 1. STATISTICS OF THE BIOPHYSICAL DESCRIPTORS BY LULC TYPE, AND THEIR CORRELATIONS WITH LST (SIGNIFICANT AT 0.05 LEVEL)

| Land-use Land-cover Type | Mean LST (Standard Deviation) | Mean Vegetation Cover (Standard Deviation) | Mean Impervious Surface (Standard Deviation) | Mean Soil Fraction (Standard Deviation) | LST/GV Fraction | LST/Impervious Surface |
|---|---|---|---|---|---|---|
| Commercial and Industrial | 305.29 (3.10) | 0.119 (0.14) | 0.491 (0.226) | 0.101 (0.234) | −0.6559 | 0.5254 |
| Residential | 303.80 (1.94) | 0.276 (0.155) | 0.254 (0.098) | 0.147 (0.144) | −0.6763 | 0.5373 |
| Cropland | 299.47 (1.28) | 0.248 (0.333) | 0.129 (0.045) | 0.3 (0.252) | −0.7538 | 0.5558 |
| Grassland | 300.47 (1.56) | 0.37 (0.198) | 0.112 (0.045) | 0.211 (0.145) | −0.3760 | 0.4742 |
| Pasture | 299.45 (1.04) | 0.258 (0.166) | 0.138 (0.097) | 0.373 (0.146) | −0.4105 | 0.5890 |
| Forest | 298.16 (1.37) | 0.715 (0.104) | 0.057 (0.030) | 0.01 (0.077) | −0.7343 | 0.3267 |
| Water | 298.20 (4.43) | 0.161 (0.178) | −0.029 (0.090) | −0.109 (0.156) | −0.2416 | 0.3538 |

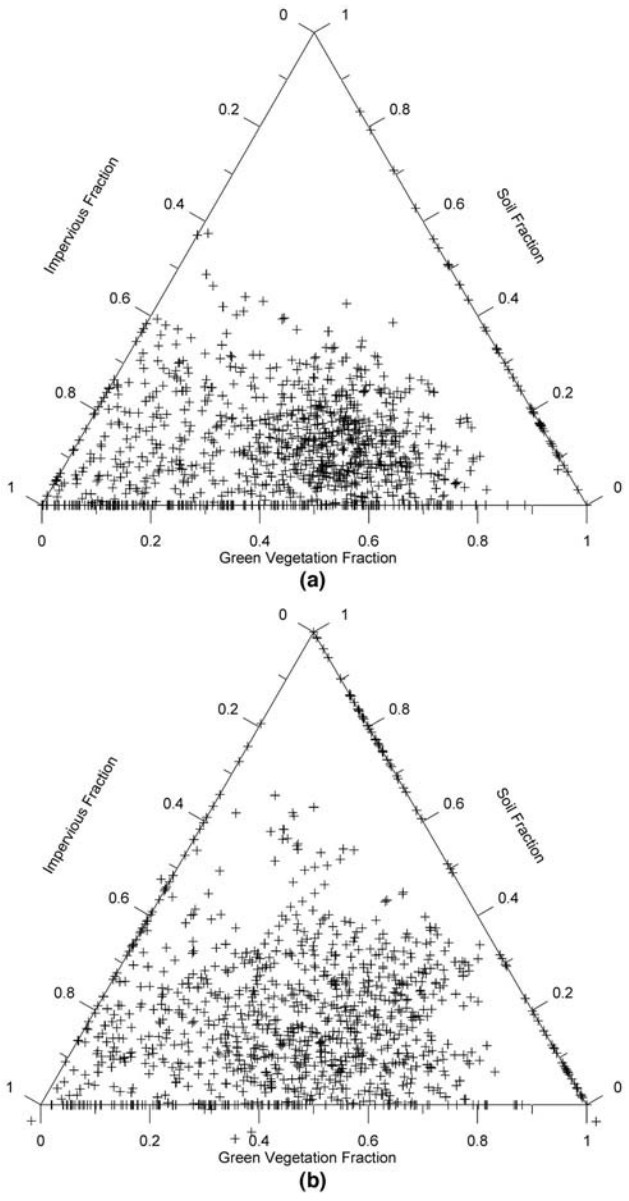


Figure 6. V-I-S composition along sampled transects: (a) Sample 1: west to east transect, and (b) Sample 2: north to south transect.

GV fraction value from 0.0 to 0.8, and impervious fraction value ranged between 0 and 1. Soil fraction values were below 0.65. When mean signature values of the fractions of each LULC type is plotted (Figure 7), quantitative relationships among the LULC types in terms of the V-I-S composition can be examined. Our current research includes examining the use of multi-temporal remote sensing data for urban time-space modeling and comparison of urban morphology in different geographical settings.

### LST and Urban Surface Biophysical Descriptors

Calculated values of LST ranged from 289.63 K to 319.02 K, with a mean of 302.14 K and standard deviation of 3.24 K. Previous remote sensing studies have demonstrated that LULC changes, especially urban development, can alter the patterns of LSTs (Weng, 2001). Since changes in LULC would lead to changes in the composition of image fractions, it is reasonable to think that the magnitude and spatial distribution of each fraction image are related to the pattern of surface temperatures. Correlation analysis was therefore

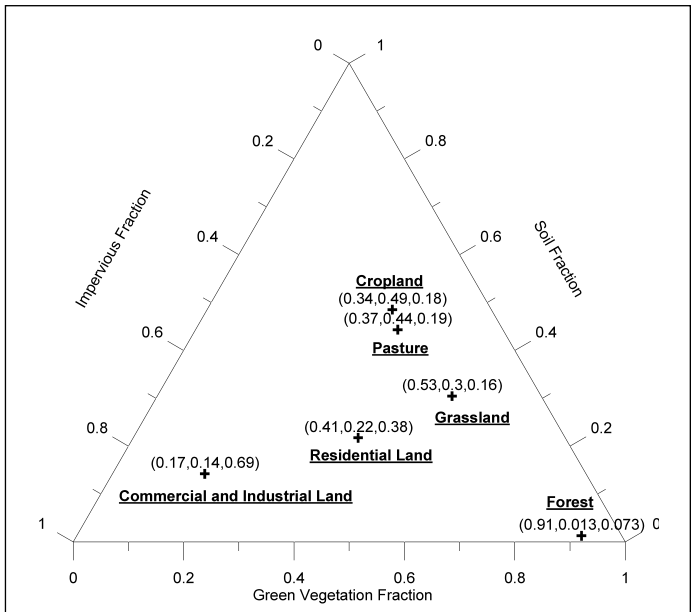


Figure 7. Quantitative relationships among the LULC types in respect to the V-I-S model. The order of the variables within the parenthesis associated with each LULC type: vegetation, soil, and impervious surface fractions.

conducted between the LST map with GV and impervious surface faction images by using all pixels in the images as observation units. The significance of each correlation coefficient was determined using a one-tail Student's t-test. Results indicate that LST was positively correlated with impervious surface fraction (coefficient = 0.5704), but negatively correlate with GV fraction (coefficient = −0.4629). If negative values for each GV and impervious surface fraction were rounded to zero, the associations between LST and the two fractions would become closer. Correlation coefficients between LST and impervious surface would reach 0.5789, whereas the relationship between LST and GV fraction would improve to a higher level of negative correlation with a coefficient of −0.5239. These relationships of LST with GV and impervious surface fractions suggest that both vegetation cover and impervious surface fractions contributed to the spatial variations of LSTs. As impervious surface is usually inversely related to vegetation cover in urban areas, LST tends to increase as vegetation cover decreases and impervious cover increases in a pixel.

To understand better the relationship between LST and urban surface biophysical descriptors, mean and standard deviation values of LST, impervious fraction, and vegetation fraction by LULC type were obtained by superimposing LULC image with the images of LST, impervious, and GV fractions. The result of the GIS overlays is shown in Table 1. It is clear that commercial and industrial land exhibited the highest temperature followed by residential land. The lowest temperature was observed in forest followed by water bodies. This implies that urban development brought up LST by approximately 6 K by replacing natural environment (forest and water) with commercial, industrial, or residential uses. The standard deviation value of LST was large for commercial and industrial land, indicating that these surfaces experienced a wide variation in LST because of different construction materials and the possibility to contain much larger buildings and a wide range of building sizes within the IFOV. In contrast, the standard deviation value of LST was relatively small for residential land owing to their homogeneity. Residential land also possessed a smaller mean value than commercial and industrial land, where buildings were frequently mixed with forest and grassland. Grassland had a median LST value, as it combined sparse vegetation and exposed bare soil. Similarly, pasture and agricultural land had a median LST value. Forests showed a considerably lower LST, because dense vegetation can reduce amount of heat stored in the soil and surface structures through transpiration. All vegetative cover, regardless of natural or man-made, exhibited an extremely small temperature variation. Water tended to get warm slowly during the summer owning to its rather high thermal inertia, and to convection and turbulence (e.g., wave action). Different water bodies (e.g., rivers, lakes, reservoirs, and ponds) exhibited different LSTs, subject to the impact of the size and depth of the water body and whether there is a flow of water through the body.

The demonstrated relationship between LULC and the three biophysical parameters, LST, GV, and impervious surface fractions suggests that it would be helpful to investigate the interplay of these environmental variables by LULC type. A pixel-by-pixel correlation analysis was conducted by computing Pearson's correlation coefficients between LST and GV fraction, and between LST and impervious surface fraction. Results are displayed in the last two columns of Table 1. For all LULC types, LST values were negatively correlated with GV fraction values, but were positively correlated with impervious fraction values. The strongest negative correlation existed between LST and GV fraction values in agricultural land and forest. The correlation coefficient values dropped slightly for residential, and commercial and industrial land, with a sharp decrease for pasture and grassland. The least correlation was found in water. On the other hand, the strongest positive correlation between LST and impervious fraction values was found in pasture and agricultural land, followed by residential land, commercial and industrial land, and grassland. The weakest correlations were observed in forestland and water.

#### LST Variations at the Census Block Groups

Census blocks, block groups, and tracts are basic units designed for population and socioeconomic census in the United States, and are widely used in urban planning and environmental management practices. In order to assess the environmental consequences of planning decisions and to facilitate environmental governance, LST and urban biophysical descriptors should be examined at the levels of census units. Remote sensing data can then be integrated with population and socioeconomic census in a GIS environment. To this end, mean LSTs were computed for each census block group, so were minimum, maximum, and standard deviation values (Figure 8). Mean values of the urban biophysical descriptors (including GV, impervious surface, and soil fractions) and the composition of LULC types in the census block groups were also calculated to elucidate further the relationships between LSTs and the these environmental variables. Similarly, remote sensing derived variables, namely, NDVI and principal component 2 (derived from the six spectral bands), were included as potential explanatory variables for LST spatial variability, since they have been demonstrated to correlate significantly with LSTs at the pixel level. Given the significance of various types of impervious surface in urban surface energy exchange, GIS data layers of building footprints and pavements were obtained to create four imperviousness variables: (a) areal percentage of pavement in the census block groups; (b) areal percentage of all buildings; (c) areal percentage of residential buildings; and (d) areal percentage of commercial and industry buildings. Finally, population density per census block group was computed as a surrogate variable of anthropogenic heat, which relates to automobiles, air conditioning units, air pollution, and heat loss from buildings. These four groups of variables (Table 2) have been identified as major factors

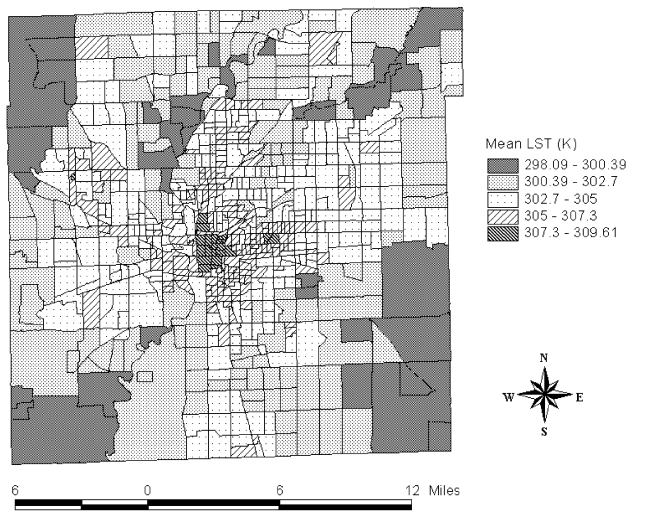


Figure 8. Mean land surface temperature by block group. Data are classified into five equal intervals.

TABLE 2. CORRELATION OF MEAN, MAXIMUM, MINIMUM, AND STANDARD DEVIATION OF LST PER BLOCK GROUP AND SELECTED EXPLANATORY VARIABLES (SIGNIFICANT AT 0.05 LEVEL)

| Categories of Variables | Variables | Mean LST | Max. LST | Min. LST | Std Dev. |
|---|---|---|---|---|---|
| LULC Composition | Per_Crop | −0.361 | −0.042 | −0.178 | −0.045 |
| | Per_Water | −0.265 | 0.09 | −0.313 | 0.465 |
| | Per_Past | −0.339 | −0.029 | −0.178 | −0.049 |
| | Per_Fore | −0.719 | −0.119 | −0.413 | 0.279 |
| | Per_Comind | 0.510 | 0.448 | 0.04 | 0.296 |
| | Per_Resi | 0.293 | −0.341 | 0.47 | −0.615 |
| | Per_Grass | −0.724 | −0.081 | −0.502 | 0.351 |
| Remote Sensing Derived Biophysical Variables | Per_Veg | −0.58 | −0.406 | −0.125 | −0.069 |
| | Per_Imper | 0.944 | 0.202 | 0.587 | −0.293 |
| | Mean_NDVI | −0.801 | −0.365 | −0.34 | 0.008 |
| | Mean_PCA | −0.709 | −0.21 | −0.44 | 0.039 |
| GIS-based Imperviousness Variables | Per_Rok | 0.709 | −0.214 | 0.684 | −0.56 |
| | Bldg_BG | 0.853 | 0.116 | 0.623 | −0.369 |
| | Per_Rear | 0.476 | −0.324 | 0.602 | −0.639 |
| | Per_Comind | 0.594 | 0.465 | 0.145 | 0.212 |
| Population Density from Census | Pop_Sqkm | 0.547 | −0.216 | 0.587 | −0.569 |

Note: PER_CROPL: percentage of cropland per blockgroup;
PER_WATER: percentage of water per blockgroup;
PER_PAST: percentage of pasture per blockgroup;
PER_FORE: percentage of forest per blockgroup;
PER_COID: percentage of commercial and industry per blockgroup;
PER_RESI: percentage of residential per blockgroup;
PER_GRAS: percentage of grassland per blockgroup.
Pop_Sqkm: population density;
Per_Imper: percentage of impervious surface;
Bldg_BG: percentage of building area;
Per_NDVI: percentage of NDVI;
Per_PCA: percentage of PCA;
PER_Rok: percentage of pavement area;
Per_REAR: percentage of residential building area;
PER_ComInd: percentage of commercial and industry building area;
PER_VEG: percentage of vegetation.

TABLE 3. STEPWISE MULTIPLE REGRESSION MODEL BETWEEN MEAN LST AND DATA EXTRACTED FROM LULC IMAGE

| | Un-standardized Coefficients | | Standardized Coefficients | | |
|---|---|---|---|---|---|
| Model | B | Std. Error | Beta | t | Sig. |
| Constant | 305.541 | .061 | | 5004.925 | .000 |
| PER_GRAS | −7.839E-02 | .003 | −.529 | −29.489 | .000 |
| PER_CROP | −8.840E-02 | .021 | −.214 | −4.164 | .000 |
| PER_FORE | −7.233E-02 | .005 | −.271 | −15.243 | .000 |
| PER_WATE | −.104 | .006 | −.247 | −17.453 | .000 |
| PER_COID | 1.897E-02 | .001 | .223 | 14.692 | .000 |
| PER_PAST | −7.056E-02 | .028 | −.127 | −2.504 | .013 |

contributing to LST variations and thus the urban heat island effect (Oke, 1982), and are therefore appropriate for LST modeling.

Relationships between mean, maximum, minimum, and standard deviation values of LST per block group and the variables identified were initially examined by correlation analysis. Table 2 shows the Pearson's correlation coefficients, which are significant at the 0.05 level as determined by a one-tail Student's t-test. Mean LST values were found negatively correlated to all vegetation related variables, but positively to imperviousness related variables, regardless the remote sensing derived biophysical measurements or those reflecting the LULC composition. Furthermore, a positive correlation was detected between LST values and all GIS derived imperviousness variables. The areal percentages of all buildings in the block group exhibited the strongest correlation, trailed by the areal percentages of pavement. The correlation of imperviousness with LST became weaker when buildings were separated into residential and commercial/industrial ones. Population density from Census 2000 was discovered to have moderately positively correlated with LST (coefficient: 0.547). Clearly, housing structure and pavement pattern possessed more explanatory power over the LST variations than population distribution.

The significant correlations between LST and the identified variables promise a potential success for using multivariate regression models to assess the relative importance of different factors underlying the urban LST variations and to identify most significant factors for prediction. A stepwise multiple regression model was built for examining the relationship between mean LST values and the areal proportions of each LULC types in each census block group (Table 3). This regression model produced a multiple coefficient of determination of 0.878 at a significant level of

TABLE 4. STEPWISE MULTIPLE REGRESSION MODEL BETWEEN MEAN LST AND OTHER DATA

| Model | Un-standardized Coefficients | | Standardized Coefficients | | |
|---|---|---|---|---|---|
| | B | Std. Error | Beta | t | Sig. |
| Constant | 298.708 | .229 | | 1305.348 | .000 |
| MEAN_IMP | 8.916E-03 | .001 | .517 | 17.790 | .000 |
| BLDG_BG | 11.271 | .873 | .360 | 12.917 | .000 |
| PER_VEG | −2.428 | .414 | −.100 | −5.862 | .000 |
| PER_ROK | 7.737E-02 | .011 | .126 | 6.916 | .000 |
| PER_REAR | −3.436E-02 | .009 | −.100 | −3.855 | .000 |
| POP00_SQMI | 3.312E-05 | .000 | .051 | 2.308 | .021 |

0.01. All LULC variables were included in the model, except for the areal proportion of residential land-use. This result indicates that LST values were associated with LULC characteristics at the block group level. Therefore, changes in LULC composition in these units will lead to changes in LST pattern and the surface energy balance. Another stepwise multiple regression model was constructed to correlate mean LST values per census block group with all non-LULC composition variables, including remote sensing derived biophysical variables, GIS-based imperviousness variables, and population density. The modeling results are shown in Table 4. The multiple regression model yielded a multiple coefficient of determination of 0.927 at a significant level of 0.02, indicating that LST had a stronger relationship with these variables than with the LULC compositions. Three variables that did not enter the model were NDVI, principal component 2, and the areal percentage of commercial and industry buildings. The most significant variable was impervious fraction, followed by the areal percentage of all buildings, both of which had a positive relationship with mean LST. Other variables possessed substantially smaller correlation coefficients. It is concluded that LST had a more direct relationship with imperviousness related variables than vegetation related variables and population density.

Geographically referenced, statistical models may be built based on the composition of LULC types within a census unit, because the spatial arrangement and areal extent of different LULC types regulate largely the variations of spectral radiance and texture in LST (Weng *et al.*, 2004). With the presence of a surface energy balance model, the spatial variations of LST may be modeled based on such factors as imperviousness, green vegetation coverage and abundance, and population density, which have been identified to relate directly or indirectly to the radiative, thermal, moisture, and aerodynamic properties in the urban surface and subsurface. This is because thermal spectral response for each pixel and therefore the thermal signature for each LULC type are largely controlled by the dynamic relationship between vegetative abundance and impervious surface coverage. This dynamics would produce an aggregated effect on the surface energy balance for each census unit. Population distribution, closely related to land-use zoning, affects the generation of anthropogenic heat and thus yields an impact on the surface energy exchange.

## Discussion and Conclusions

The need is apparent for developing and applying quantitative surface descriptors to describe urban thermal landscapes in remote sensing studies. To make these happen, remote sensing techniques must enable a parsimonious separation of urban LULC types into values directly related to their scale and signature (Phinn *et al.*, 2002). This study has demonstrated that SMA, based on the V-I-S model, can provide a physically based solution for characterizing and quantifying urban landscape compositions, and that SMA-derived fraction estimates can be used as reliable urban surface biophysical descriptors. Moreover, since image endmembers were utilized in this research, they were capable of representing the spectra measured at the same scale as the image data. Thus, pixel-based LST measurements were able to relate effectively to the biophysical descriptors. A linkage between the two types of data has made it possible for an analysis of the causes of LST variations in Indianapolis.

Simple correlations between pixel-based thematic LULC data and the thermal signatures were criticized for impeding progress towards a better understanding of urban thermal landscapes and the urban heat island phenomena (Voogt and Oke, 2003). As a comparison, this study has examined the relationship between LST values and the compositions of LULC types within the census block groups, as well as the relationships between LST and the urban biophysical descriptors derived from SMA, and other relevant spatial data. Results indicate that LST possessed a stronger relationship with these variables than with the LULC compositions.

This study demonstrates that SMA provides a suitable model to decompose the spectral mixtures of L-resolution data such as Landsat TM/ETM+. The scene elements in the L-resolution data are smaller than the resolution cell of the sensor, and are therefore not detectable (Strahler *et al.*, 1986). Thus, a more realistic representation and quantification of urban surfaces are possible, in comparison to that provided by the assignment of a single dominant class to every pixel by statistical models. With the availability of multi-temporal satellite images, stable and reliable fraction estimates derived from SMA may be more effective for a LULC change detection than traditional pixel-by-pixel comparison methods, because the fractional characteristics of LULC types at one date are comparable with other dates of fraction images. Fraction images may also be easily translated into significant environmental variables such as impervious surface and vegetation abundance. By relating LST to changing fraction constituency over time with urban growth, the effect of urbanization on LST may be examined.

SMA, as a remote sensing analytical procedure for the V-I-S model, needs to be refined in order to objectively characterize urban morphology and to examine the environmental consequences. Because of the complexity of impervious surface, urban areas may have substantially different impervious surfaces. Identifying a suitable endmember to represent all types of impervious surfaces is challenging. Moreover, impervious surfaces tend to be confused with dry soils. On the other hand, shade is an important component captured by optical remote sensors, which is not included in the V-I-S model. Three possible approaches may be taken to overcome these problems: by stratification of the image, by use of

multiple endmembers, and by use of hyperspectral imagery. More endmembers require more spectral bands to be used, since the maximum number of endmembers is directly proportional to the number of spectral bands. The vastly increased dimensionality of a hyperspectral sensor can effectively remove the sensor-related limit on the number of endmembers available. More significantly, the fact that the number of hyperspectral image channels far exceeds the likely number of endmembers for most applications readily permits the exclusion from the analysis of any bands with low signal-to-noise ratios or with significant atmospheric absorption effects (Lillesand *et al.*, 2004, p. 614). In addition, a multiple-endmember SMA approach has shown a better performance than a standard SMA approach, when a large number of endmembers are required to be modeled across a scene (Painter *et al.*, 1998; Roberts *et al.*, 1998b; Okin *et al.*, 2001).

## Acknowledgments

This research is supported by National Science Foundation (BCS-0521734) for a project entitled "Role of Urban Canopy Composition and Structure in Determining Heat Islands: A Synthesis of Remote Sensing and Landscape Ecology Approach," by NASA through Indiana Space Grant Consortium (NGTS-40114-4) for a project entitled "A Seasonal Analysis of Satellite Detected Urban Heat Island Phenomenon in Indianapolis," and by the University Research Committee of Indiana State University (UNR184). We would also like to thank three anonymous reviewers for their constructive comments and suggestions.

## References

Adams, J.B., D.E. Sabol, V. Kapos, R.A. Filho, D.A. Roberts, M.O. Smith, and A.R. Gillespie, 1995. Classification of multispectral images based on fractions of endmembers: Application to land cover change in the Brazilian Amazon, *Remote Sensing of Environment*, 52:137–154.

Artis, D.A., and W.H. Carnahan, 1982. Survey of emissivity variability in thermography of urban areas, *Remote Sensing of Environment*, 12:313–329.

Arvidson, T., 2002. Personal Correspondence, Landsat-7 Senior Systems Engineer, Landsat Project Science Office, Goddard Space Flight Center, Washington, D.C.

Brun, S.E., and L.E. Band, 2000. Simulating runoff behavior in an urbanizing watershed, *Computers, Environment and Urban Systems*, 24:5–22.

Campbell, J.B., 2002. *Introduction to Remote Sensing*, 3rd edition, The Guilford Press, New York, New York, 621 p.

Carnahan, W.H., and R.C. Larson, 1990. An analysis of an urban heat sink, *Remote Sensing of Environment*, 33:65–71.

Caselles, V., J.A. Sobrino, and C. Coll, 1992a. On the use of satellite thermal data for determining evapotranspiration in partially vegetated areas, *International Journal of Remote Sensing*, 13:2669–2682.

Caselles, V., J.A. Sobrino, and C. Coll, 1992b. A physical model for interpreting the land surface temperature obtained by remote sensors over incomplete canopies, *Remote Sensing of Environment*, 39:203–211.

Clapham, W.B. Jr., 2003. Continuum-based classification of remotely sensed imagery to describe urban sprawl on a watershed scale, *Remote Sensing of Environment*, 86:322–340.

Dash, P., F.-M. Gottsche, F.-S. Olesen, and H. Fischer, 2002. Land surface temperature and emissivity estimation from passive sensor data: Theory and practice-current trends, *International Journal of Remote Sensing*, 23:2563–2594.

Goward, S.N., 1981. Thermal behavior or urban landscapes and the urban heat island, *Physical Geography*, 1(2):19–33.

Goward, S.N., Y. Xue, and K.P. Czajkowski, 2002. Evaluating land surface moisture conditions from the remotely sensed temperature/vegetation index measurements: An exploration with the simplified simple biosphere model, *Remote Sensing of Environment*, 79:225–242.

Jasinski, M.F., 1990. Sensitivity of the Normalized Difference Vegetation Index to subpixel canopy cover, soil albedo, and pixel scale, *Remote Sensing of Environment*, 32:169–187.

Landsat Project Science Office, 2002. *Landsat 7 Science Data User's Handbook*, Goddard Space Flight Center, NASA, Washington, D.C., URL: http://ltpwww.gsfc.nasa.gov/IAS/handbook/handbook_toc.html (last date accessed: 15 August 2006).

Larson, R.C., and W.H. Carnahan, 1997. The influence of surface characteristics on urban radiant temperatures, *Geocarto International*, 12:5–16.

Lillesand, T.M., R.W. Kiefer, and J.W. Chipman, 2004. *Remote Sesning and Image Interpretation*, John Wiley and Sons, New York, p. 614.

Lu, D., and Q. Weng, 2004. Spectral mixture analysis of the urban landscapes in Indianapolis city with Landsat ETM+ Imagery, *Photogrammetric Engineering & Remote Sensing*, 70:1053–1062.

Madhavan, B.B., S. Kubo, N. Kurisaki, and T.V.L.N. Sivakumar, 2001. Appraising the anatomy and spatial growth of the Bangkok Metropolitan area using a vegetation-impervious-soil model through remote sensing, *International Journal of Remote Sensing*, 22:789–806.

Markham, B.L., and J.L. Barker, 1987. Thematic Mapper bandpass solar exoatmospheric irradiances, *International Journal of Remote Sensing*, 8:517–523.

Mustard, J.F., and J.M. Sunshine, 1999. Spectral analysis for earth science: Investigations using remote sensing data, *Remote Sensing for the Earth Sciences: Manual of Remote Sensing*, (A.N. Rencz, editor), Volume 3, John Wiley and Sons, New York, pp. 251–307.

Nichol, J.E., 1996. High-resolution surface temperature patterns related to urban morphology in a tropical city: A satellite-based study, *Journal of Applied Meteorology*, 35:135–146.

Oke, T.R., 1982. The energetic basis of the urban heat island, *Quarterly Journal of the Royal Meteorological Society*, 108:1–24.

Okin, G.S., D.A. Roberts, B. Murray, and W.J. Okin, 2001. Practical limits on hyperspectral vegetation discrimination in arid and semiarid environments, *Remote Sensing of Environment*, 77:212–225.

Owen, T.W., T.N. Carlson, and R.R. Gillies, 1998. An assessment of satellite remotely-sensed land cover parameters in quantitatively describing the climatic effect of urbanization, *International Journal of Remote Sensing*, 19:1663–1681.

Painter, T.H., D.A. Roberts, R.O. Green, and J. Dozier, 1998. The effects of grain size on spectral mixture analysis of snow-covered area from AVIRIS data, *Remote Sensing of Environment*, 65:320–332.

Phinn, S., M. Stanford, P. Scarth, A.T. Murray, and P.T. Shyy, 2002. Monitoring the composition of urban environments based on the vegetation-impervious surface-soil (VIS) model by subpixel analysis techniques, *International Journal of Remote Sensing*, 23:4131–4153.

Prata, A.J., V. Caselles, C. Coll, J.A. Sobrino, and C. Ottle, 1995. Thermal remote sensing of land surface temperature from satellites: Current status and future prospects, *Remote Sensing Reviews*, 12:175–224.

Rashed, T., J.R. Weeks, M.S. Gadalla, and A.G. Hill, 2001. Revealing the anatomy of cities through spectral mixture analysis of multisepctral satellite imagery: A case study of the Greater Cairo region, Egypt, *Geocarto International*, 16:5–15.

Ridd, M.K., 1995. Exploring a V-I-S (Vegetation-Impervious Surface-Soil) model for urban ecosystem analysis through remote sensing: comparative anatomy for cities, *International Journal of Remote Sensing*, 16:2165–2185.

Roberts, D.A., G.T. Batista, J.L.G. Pereira, E.K. Waller, and B.W. Nelson, 1998a. Change identification using multitemporal spectral mixture analysis: Applications in eastern Amazônia, *Remote Sensing Change Detection: Environmental Monitoring Methods and Applications* (R.S. Lunetta and C.D. Elvidge, editors), Ann Arbor Press, Ann Arbor, Michigan, pp. 137–161.

Roberts, D.A., M. Gardner, R. Church, S. Ustin, G. Scheer, and R.O. Green, 1998b, Mapping chaparral in the Santa Monica mountains using multiple endmember spectral mixture models, *Remote Sensing of Environment*, 65:267–279.

Sandholt, I., K. Rasmussen, and J. Andersen, 2002. A simple interpretation of the surface temperature/vegetation index space for assessment of surface moisture status, *Remote Sensing of Environment*, 79:213–224.

Schueler, T.R., 1994. The importance of imperviousness, *Watershed Protection Techniques*, 1(3):100–111.

Small, C., 2001. Estimation of urban vegetation abundance by spectral mixture analysis, *International Journal of Remote Sensing*, 22:1305–1334.

Snyder, W.C., Z. Wan, Y. Zhang, and Y.-Z. Feng, 1998. Classification-based emissivity for land surface temperature measurement from space, *International Journal of Remote Sensing*, 19: 2753–2774.

Soil Conservation Service, 1975. Urban Hydrology for Small Watersheds, *USDA Soil Conservation Service Technical Release No. 55*, Washington, D.C.

Strahler, A.H., C.E. Woodcock, and J.A. Smith, 1986. On the nature of models in remote sensing, *Remote Sensing of Environment*, 70:121–139.

Voogt, J.A., and T.R. Oke, 1998. Effects of urban surface geometry on remotely-sensed surface temperature, *International Journal of Remote Sensing*, 19:895–920.

Voogt, J.A., and T.R. Oke, 2003. Thermal remote sensing of urban climate, *Remote Sensing of Environment*, 86:370–384.

Ward, D., S.R. Phinn, and A.L. Murray, 2000. Monitoring growth in rapidly urbanizing areas using remotely sensed data, *Professional Geographer*, 53:371–386.

Weng, Q., 2001. A remote sensing-GIS evaluation of urban expansion and its impact on surface temperature in the Zhujiang Delta, China, *International Journal of Remote Sensing*, 22:1999–2014.

Weng, Q., D. Lu, and J. Schubring, 2004. Estimation of land surface temperature-vegetation abundance relationship for urban heat island studies, *Remote Sensing of Environment*, 89:467–483.

Wu, C., and A.T. Murray, 2003. Estimating impervious surface distribution by spectral mixture analysis, *Remote Sensing of Environment*, 84:493–505.

(Received 23 June 2005; accepted 25 July 2005; revised 20 September 2005)